Nanocluster

DOI: 10.1002/ange.201402685

Magnetic and Optoelectronic Properties of Gold Nanocluster–Thiophene Assembly**

*Wei Qin, Jessica Lohrman, and Shenqiang Ren**

Abstract: *Nanohybrids consisting of Au nanocluster and polythiophene nanowire assemblies exhibit unique thermal-responsive optical behaviors and charge-transfer controlled magnetic and optoelectronic properties. The ultrasmall Au nanocluster enhanced photoabsorption and conductivity effectively improves the photocurrent of nanohybrid based photovoltaics, leading to an increase of power conversion efficiency by 14 % under AM 1.5 illumination. In addition, nanohybrids exhibit electric field controlled spin resonance and magnetic field sensing behaviors, which open up the potential of charge-transfer complex system where the magnetism and optoelectronics interact.*

Multifunctional polymeric materials have attracted much interests due to their broad technological applications, such as optoelectronics,[1] thermoelectrics,[2] and sensors.[3] Recently, the co-existence of ferroelectricity and ferromagnetism in polymeric multiferroics opens up a host of new functionalities that are absent in each of the individual component,[4] such as the magnetoelectric (ME) coupling or optically tunable ME effects. The room temperature ME effects of charge-transfer materials are currently focused on the organic complex materials, such as organic semiconducting poly(9-vinylcarbazole):1,2,4,5-tetrachloro-3-nitrobenzene donor–acceptor systems.[5] In addition, supramolecular charge-transfer complexes result in the formation of dipoles that can exhibit ferroelectricity due to a collective transfer of electrons from donor to acceptor.[6] Compared to all organic charge-transfer complex systems, ultrasmall noble metal nanoclusters as electron acceptors could provide the control of charge-transfer induced multifunctionalities, due to their tunable band structures by alteration of the nanoclusters size.[7]

Ultrasmall noble metal nanoclusters (i.e., with diameters less than 2.5 nm) are considered to be semiconducting quasi-molecules and their physical and chemical properties are distinct from their metal counterparts.[8] The optical transition of metal nanoclusters confirms that their band gaps are well structured between the highest occupied molecular orbital (HOMO) and the lowest unoccupied molecular orbital (LUMO).[7a,9] The band gap (ranging from 0.1 eV to 2 eV) can be tuned by changing the size of nanoclusters, and it will vanish at bigger nanocluster sizes.[7b,c] Nanoclusters have been reported with sizes smaller than the 2.5 nm,[10] and therefore, are suitably sized for becoming a promising candidate as the acceptor material in charge-transfer complex systems.

Here, we report Au nanocluster (acceptor)–crystalline polymer (donor) material (Au:P3HT nanohybrid; P3HT = poly(3-hexylthiophene-2,5-diyl) with a focus on its charge-transfer dependent spin resonance, magnetic, and optoelectronic properties. By tuning Au nanocluster ratios, we show the controllable photoabsorption, magnetism and electric field dependent susceptibility of charge-transfer nanohybrids. Au nanocluster enhanced photoabsorption and conductivity significantly improves power conversion efficiency (14 % increase) of the nanohybrid-based photovoltaics. Moreover, the ME coupling effect and magnetic field sensing behavior of Au:P3HT nanohybrids is shown by tuning the ratio between singlet and triplet charge-transfer states.

Block copolymers have been utilized as the nanoreactor to synthesize and self-assemble periodic nanocluster features. In this work, to control the size and ratio of Au nanoclusters, we apply block copolymer polystyrene-*b*-poly(4-vinylpyridine) (PS-*b*-P4VP) to synthesize and assemble Au nanoclusters due to the electrostatic interaction of the pyridine moiety and the gold complexes. The ratio between PS and P4VP blocks dictate the Au nanocluster distribution and its geometry within the P4VP domain. The resulting Au nanoclusters are embedded into the P4VP domain which can prevent them from aggregating into metallic Au nanoparticles. The average size of Au nanoclusters can be tuned from 1 nm to 2.2 nm by controlling the $HAuCl_4$ loading concentration, which has been confirmed in our previous work.[10] Due to the thiophene nanowire backbone and hexal–hexal spacing, the Au nanocluster (average size 1.9 nm) selectively interacts with P3HT nanowires to form the charge-transfer nanohybrids. The schematic Au:P3HT nanohybrids (Figure 1 a) indicate self-assembly and the distribution of Au nanoclusters and P3HT nanowires, which is confirmed by the TEM image as shown in Figure 1 b. By increasing the Au nanocluster loadings, the nanohybrid solution becomes darker due to a red shift in the photoabsorption (Figure 1 c). It should be noted that the photoexcitation can initiate charge-transfer between semiconducting Au nanoclusters and P3HT nanowires. The photoabsorption spectra of Au:P3HT nanohybrids, with different ratios, are shown in Figure 1 d. By increasing the loading ratio of Au nanoclusters, the NIR photoabsorption becomes more pronounced. Considering that electrons can be directly excited from donor to acceptor,[11] an increased Au nanocluster loading will enable more electrons to be excited from the P3HT nanowire to the Au nanocluster, which significantly enhances the NIR photo-

[*] Dr. W. Qin, J. Lohrman, Prof. S. Ren
Department of Chemistry, University of Kansas
Lawrence, KS 66045 (USA)
E-mail: shenqiang@ku.edu

[**] S.R. thanks the financial support from US Department of Energy award (DE-FG02-13ER46937).

Supporting information for this article is available on the WWW under http://dx.doi.org/10.1002/anie.201402685.

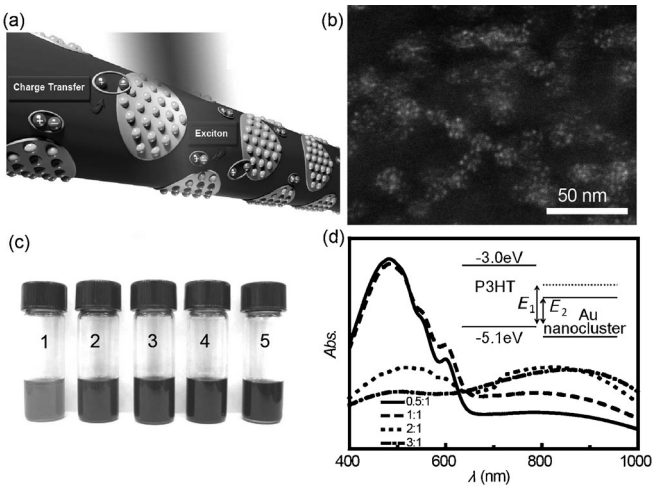

Figure 1. a) Au nanocluster:P3HT nanowire complex. b) TEM image of Au:P3HT nanohybrids, in which the Au nanoclusters are arranged into the P4VP domain. c) Vial 1: P3HT solution; vial 2: P3HT nanowire solution; vials 3–5: Au:P3HT nanohybrid solutions at 0.5:1, 1:1, and 2:1 ratio, respectively. d) Photoabsorption spectra of Au:P3HT nanohybrids at different loading ratios. The inset shows the size effect of Au nanoclusters on the LUMO level.

absorption. The absorption peaks at 780 nm, 800 nm, 820 nm and 850 nm are corresponding to Au:P3HT ratios of 0.5:1, 1:1, 2:1 and 3:1, respectively. A larger size of Au nanoclusters could yield a smaller band gap. As shown in the inset of Figure 1 d, as the Au nanocluster band gap becomes smaller, it needs less energy ($E_2 < E_1$) to excite electrons from the donor's HOMO to the acceptor's LUMO, which is responsible for the red-shift of the absorption spectra by increasing the Au nanocluster loading ratio.

To fine-tune the charge-transfer states, we thermally manipulate the distance between Au nanoclusters and P3HT nanowires. As shown in Figure 2 a, the charge-transfer induced absorption of the Au:P3HT nanohybrid exhibits a reversible behavior under heating–cooling cycles, due to the thermally induced distance extension from the Au nanocluster to the P3HT nanowires (Figure 2 b). As shown in the inset of Figure 2 a, R is the radius of P3HT nanowire, and r represents the distance between the P3HT nanowire and the Au nanocluster tuned by temperature. The charge-transfer induced built-in electric field between the P3HT nanowire and the Au nanocluster (hole in P3HT nanowire and electron in Au nanocluster) can be expressed as:

$$E = \frac{\eta}{2\pi\varepsilon_0\varepsilon_r}\frac{1}{r}$$

(P3HT nanowire length is considerably larger than the distance r), where η is linear density of charge of the P3HT nanowire, and ε_r is the dielectric constant. The Coulomb energy of exciting one electron form the P3HT nanowire to the Au nanocluster is shown as:

$$E_C = \frac{\eta e}{2\pi\varepsilon_0\varepsilon_r}\ln\left(\frac{r}{R}\right).$$

A larger distance, r, in Au:P3HT nanohybrids, induced by a higher temperature, would need higher energy to overcome the Coulombic interaction, which will weaken the charge-transfer absorption between the P3HT nanowire and the Au nanocluster. Therefore, the NIR absorption is suppressed under higher temperatures. In addition, the NIR absorption is not observed within the samples composed of P3HT nanowire only (see the Supporting Information).

Charge-transfer states can dissociate into free charge carriers in Au:P3HT nanohybrids. By applying a magnetic field, B, and microwave radiation on the sample, the transition between spin-up and spin-down electrons can take place, thereby allowing an electron spin resonance (ESR) that can be detected (the detailed ESR spectra is shown in the Supporting Information). For a given material, if the ESR line width is fixed, the presence of a strong ESR signal indicates a large magnetic susceptibility. As shown in Figure 3 a, the susceptibilities of Au:P3HT charge-transfer nanohybrids decrease as the temperature is increased. In most materials, the susceptibility follows Curie's law:

$$\chi \propto \frac{n_0}{T}\mu_B^2,$$

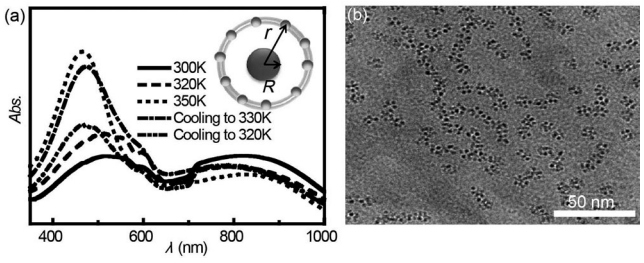

Figure 2. a) Photoabsorption spectra of Au:P3HT nanohybrids under heating and cooling. The inset shows a schematic drawing of Au nanoclusters and P3HT nanowire. b) TEM image of Au:P3HT nanohybrids after 350 K thermal annealing.

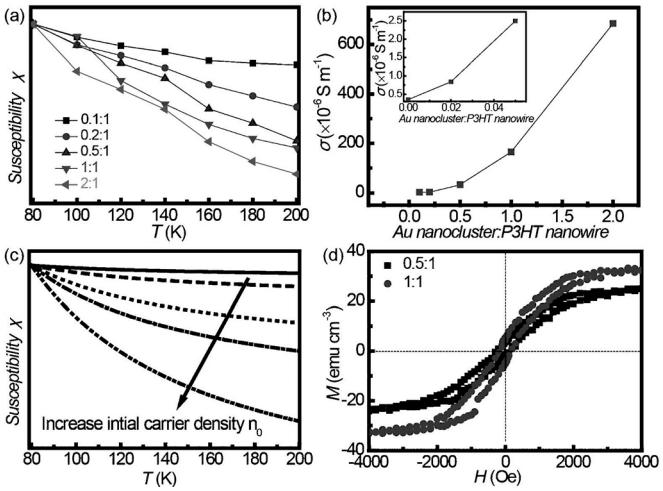

Figure 3. a) Temperature-dependent magnetic susceptibilities of Au:P3HT nanohybrids at different molar ratios. b) Conductivity as a function of the Au:P3HT ratio. c) Temperature-dependent susceptibility simulations. d) *M*–*H* loops of Au:P3HT nanohybrids at 0.5:1 and 1:1 ratios.

where n_0 is the initial carrier density. From this, it is shown that temperature can induce a decrease of susceptibility. However, taking into account the thermally excited carriers, the total susceptibility can be expressed as:

$$\chi \propto \frac{n_0 + n(T)}{T}\mu_B^2,$$

where $n(T)$ is the thermal excitation induced carrier density, which is determined by the band gap E_g of the semiconductor:

$$n(T) \propto \exp(-E_g/2k_B T).$$

It should be noted that more charge carriers will be produced by increasing the Au nanocluster acceptor ratio due to charge-transfer dissociation, which could make the initial carrier density, n_0, become larger. In semiconductor materials, the conductivity, σ, is determined by carrier mobility, μ, and carrier density, n: $\sigma = ne\mu$. Therefore, the conductivity of Au:P3HT nanohybrids increases with the Au nanocluster ratio, as shown in Figure 3b (The details of the device current–voltage performance are shown in the Supporting Information). Figure 3a shows that susceptibilities decrease faster with temperature under a larger Au nanocluster ratio due to the increased initial carrier density. Therefore, we can calculate the temperature dependent susceptibilities with different initial carrier densities, as shown in Figure 3c, which matches the experimental results well. The magnetization hysteresis (M–H) loop is shown in Figure 3d for different Au nanocluster loading ratios. A 1:1 ratio of Au nanocluster:P3HT shows a higher saturation of magnetization than that of the 0.5:1 nanohybrid, which further confirms the charge-transfer related magnetism. Singlet charge-transfer states could transfer into triplet states after applying a magnetic field.[12] Because charge-transfer is a transitional state, it will dissociate into free charge or recombine into excitons. Therefore, a higher Au nanocluster ratio in the Au:P3HT nanohybrids will induce more triplet exciton density with the effect of a magnetic field, which can contribute to the triplet excitonic ferromagnetism.[4b]

Figure 4a shows the current density–voltage (J–V) curves of organic P3HT nanowire and PCBM (phenyl-C_{61}-butyric acid methyl ester) solar cells with and without Au nanoclusters, respectively, in which the short circuit current (J_{sc}) increases when the Au nanoclusters are present. The external quantum efficiency (EQE) of the nanohybrid devices is shown in Figure 4b, in which the photocurrent at a 850 nm wavelength matches well with its charge-transfer induced NIR absorption due to the Au nanocluster loading. In addition, Au nanoclusters have a close interaction with the P3HT nanowire (as shown in the TEM image of Figure 1b). Therefore, the electron–hole (e–h) distance (hole in P3HT nanowire and electron in PCBM) increases with the loading of the Au nanoclusters, which will contribute to the photocurrent due to the increased carrier density through efficient e–h dissociation. At 0.02% loading of the Au nanoclusters, the power conversion efficiency of the organic solar cells is increased to the maximum value (Figure 4c). The aggregation by further increasing the Au nanocluster ratios will largely decrease the photocurrent (as shown in the EQE spectrum, Supporting Information).

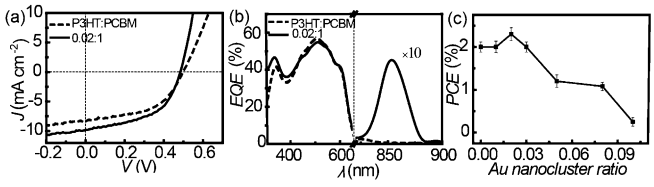

Figure 4. a) J–V curves of P3HT nanowire:PCBM and Au nanocluster loading in P3HT nanowire:PCBM (0.02:1 ratio). b) EQE spectra of nanohybrid solar cells with different Au nanocluster loading ratios. c) Power conversion efficiency of nanohybrid solar cells as a function of Au nanocluster loading ratios.

To study the magnetoelectric effect in Au:P3HT nanohybrids, electric field tunable ESR is presented, as shown in Figure 5a. A slight decrease in the spin resonance field is observed after increasing the applied electric field. In organic materials, electric fields can tune the coupling of polarons with an optical mode, an acoustic mode, or both. Therefore, the applied electric field can affect the velocity and localization of the polaron,[13] which will determine the value of the polaron g factor. From the equation of $g\mu_B B = h\nu$, where microwave frequency $\nu = 9.7$ GHz is used in measurements, it should be noted that decreasing the resonance field with an electric field means an increase of g factor. The g factor is increased from 2.004 (without electric field) to 2.007 with the applied electric field of 50 MV m^{-1} (Figure 5a). As shown in Figure 5c, both the current density and magnetic field effect are small in Au:P3HT nanohybrids. By adding the PCBM phase into Au:P3HT system, the electric field tunable ESR signal is more pronounced (as shown in Figure 5b), which is also confirmed by the high current density in the devices (Figure 5d). In addition to electric field dependent ESR, a magnetic field can also tune the ratio between singlet and

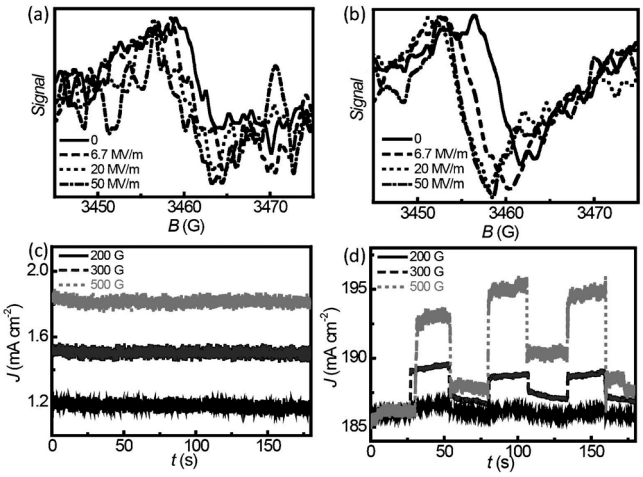

Figure 5. a,b) Electric field dependent ESR spectra of Au:P3HT nanohybrid (a) and Au:P3HT:PCBM devices (b) at room temperature. c,d) Magnetic field sensing results for Au:P3HT nanohybrid (c) and Au:P3HT:PCBM devices (d).

triplet states, which can cause magnetic field effects.[14] In particular, singlet and triplet charge-transfer states can be readily tuned by an applied magnetic field when the e–h distance is large (a larger e–h distance means a smaller exchange interaction of charge-transfer).[12] As mentioned above, Au nanoclusters could increase the e–h distance between the P3HT nanowire and the PCBM phase, leading to the pronounced magnetic field effects (Figure 5d). However, a much higher magnetic field is needed to tune singlet and triplet ratios due to a larger exchange interaction of charge-transfer (the e–h distance is small in both Au:P3HT nanohybrid and P3HT nanowire:PCBM). Therefore, the magnetic field effects of Au:P3HT nanohybrid and P3HT nanowire:PCBM is rather weak (Figure 5c and Supporting Information). The PCBM doped Au:P3HT nanohybrid system shows great promise as an organic magnetic field sensor.

In conclusion, we present optoelectronic and magnetic properties of Au:P3HT nanohybrids by controlling the charge-transfer interaction. The Au nanocluster:P3HT charge-transfer assembly enables a broad photoabsorption, which can be tuned by the size of Au nanoclusters. The thermal-responsive photoabsorption of Au:P3HT nanohybrids is controlled by the thermally tuned distance between the P3HT nanowire and Au nanoclusters. The nanohybrid photovoltaic device exhibits 14% increase of power conversion efficiency due to the Au nanocluster enhanced photoabsorption, conductivity and charge separation. The electric field controlled spin resonance and magnetic field sensing is demonstrated, which shows a great promise for the integration of optoelectronics and magnetism of charge-transfer systems.

Experimental Section

Synthesis of Au:P3HT nanohybrids: Polystyrene-*b*-poly(4-vinylpyridine) (PS-*b*-P4VP, molecular weights of PS and P4VP are 19 $kg\,mol^{-1}$ and 5.2 $kg\,mol^{-1}$, respectively) is used to reduce gold cation Au^{3+} to form Au nanoclusters. PS-*b*-P4VP (concentration 0.5 $mg\,mL^{-1}$) and $HAuCl_4$ are dissolved into tetrahydrofuran at 1:1 molar ratio. The PS-*b*-P4VP:$HAuCl_4$ solution is mixed with the crystalline thiophene nanowire solution (1,2-dichlorobenzene) at different ratios in an N_2 glovebox.

Device structure: The device consists of the following sequence of films: ITO/poly(3,4-ethylenedioxythiophene)–poly(styrenesulfonate) (PEDOT-PSS)/active layer/Al. PEDOT:PSS (Baytron PVP CH 8000) is spin cast onto a $0.5 \times 0.5\ in^2$ glass substrate with pre-patterned ITO electrodes. The nanohybrid solution is spun at 1000 rpm for 1 min, and subjected to annealing overnight in 1,2-dichlorobenzene solvent. The device was annealed at 140 °C for 10 min. The 120 nm thick Al top contact layer was evaporated at a rate of 0.1 $nm\,s^{-1}$ as the cathode, through a shadow mask to generate an array of patterned electrodes (the active photoactive area is 0.01 cm^2). The final device area was defined by the overlap between the top and bottom electrodes.

Received: February 21, 2014
Revised: March 11, 2014
Published online: May 22, 2014

Keywords: charge-transfer · gold nanocluster · magnetic field sensor · magnetoelectric effect

[1] a) H. Zheng, Y. Zheng, N. Liu, N. Ai, Q. Wang, S. Wu, J. Zhou, D. Hu, S. Yu, S. Han, W. Xu, C. Luo, Y. Meng, Z. Jiang, Y. Chen, D. Li, F. Huang, J. Wang, J. Peng, Y. Cao, *Nat. Commun.* **2013**, *4*, 1971; b) A. J. Heeger, *Adv. Mater.* **2014**, *26*, 10–28; c) Y. Yuan, T. J. Reece, P. Sharma, S. Poddar, S. Ducharme, A. Gruverman, Y. Yang, J. Huang, *Nat. Mater.* **2011**, *10*, 296–302.

[2] L. Yan, M. Shao, H. Wang, D. Dudis, A. Urbas, B. Hu, *Adv. Mater.* **2011**, *23*, 4120–4124.

[3] W. J. Baker, K. Ambal, D. P. Waters, R. Baarda, H. Morishita, K. van Schooten, D. R. McCamey, J. M. Lupton, C. Boehme, *Nat. Commun.* **2012**, *3*, 898.

[4] a) J. Jin, S. G. Lu, C. Chanthad, Q. Zhang, M. A. Haque, Q. Wang, *Adv. Mater.* **2011**, *23*, 3853–3858; b) S. Ren, M. Wuttig, *Adv. Mater.* **2012**, *24*, 724–727; c) P. Lunkenheimer, J. Müller, S. Krohns, F. Schrettle, A. Loidl, B. Hartmann, R. Rommel, M. de Souza, C. Hotta, J. A. Schlueter, M. Lang, *Nat. Mater.* **2012**, *11*, 755–758; d) A. Rajca, J. Wongsriratanakul, S. Rajca, *Science* **2001**, *294*, 1503–1505.

[5] H. Zang, L. Yan, M. Li, L. He, Z. Gai, I. Ivanov, M. Wang, L. Chiang, A. Urbas, B. Hu, *Sci. Rep.* **2013**, *3*, 2812.

[6] A. S. Tayi, A. K. Shveyd, A. C. H. Sue, J. M. Szarko, B. S. Rolczynski, D. Cao, T. J. Kennedy, A. A. Sarjeant, C. L. Stern, W. F. Paxton, W. Wu, S. K. Dey, A. C. Fahrenbach, J. R. Guest, H. Mohseni, L. X. Chen, K. L. Wang, J. F. Stoddart, S. I. Stupp, *Nature* **2012**, *488*, 485–489.

[7] a) M. Valden, X. Lai, D. W. Goodman, *Science* **1998**, *281*, 1647–1650; b) C. P. Vinod, G. U. Kulkarni, C. N. R. Rao, *Chem. Phys. Lett.* **1998**, *289*, 329–333; c) C. Xu, X. Lai, G. W. Zajac, D. W. Goodman, *Phys. Rev. B* **1997**, *56*, 13464–13482; d) R. Jin, *Nanoscale* **2010**, *2*, 343–362.

[8] a) O. M. Bakr, V. Amendola, C. M. Aikens, W. Wenseleers, R. Li, L. Dal Negro, G. C. Schatz, F. Stellacci, *Angew. Chem.* **2009**, *121*, 6035–6040; *Angew. Chem. Int. Ed.* **2009**, *48*, 5921–5926; b) W. A. de Heer, *Rev. Mod. Phys.* **1993**, *65*, 611–676; c) B. C. Gates, *Chem. Rev.* **1995**, *95*, 511–522.

[9] a) H. Häkkinen, *Chem. Soc. Rev.* **2008**, *37*, 1847–1859; b) Y. Negishi, K. Nobusada, T. Tsukuda, *J. Am. Chem. Soc.* **2005**, *127*, 5261–5270; c) R. Archana, S. Sonali, M. Deepthy, R. Prasanth, M. Habeeb, P. Thalappil, N. Shantikumar, K. Manzoor, *Nanotechnology* **2010**, *21*, 055103; d) S. Link, A. Beeby, S. FitzGerald, M. A. El-Sayed, T. G. Schaaff, R. L. Whetten, *J. Phys. Chem. B* **2002**, *106*, 3410–3415.

[10] S. Ren, S. K. Lim, S. Gradecak, *Chem. Commun.* **2010**, *46*, 6246–6248.

[11] D. V. Lopatin, V. V. Rodaev, A. V. Umrikhin, D. V. Konarev, A. L. Litvinov, R. N. Lyubovskaya, *J. Mater. Chem.* **2005**, *15*, 657–660.

[12] W. Qin, K. Gao, S. Yin, S. J. Xie, *J. Appl. Phys.* **2013**, *113*, 193901.

[13] a) X. Liu, K. Gao, J. Fu, Y. Li, J. Wei, S. Xie, *Phys. Rev. B* **2006**, *74*, 172301; b) W. Zhang, A. O. Govorov, S. E. Ulloa, *Phys. Rev. B* **2002**, *66*, 134302.

[14] a) B. Hu, L. Yan, M. Shao, *Adv. Mater.* **2009**, *21*, 1500–1516; b) B. Hu, Y. Wu, *Nat. Mater.* **2007**, *6*, 985–991; c) T. D. Nguyen, G. H. Markosian, F. Wang, L. Wojcik, X. G. Li, E. Ehrenfreund, Z. V. Vardeny, *Nat. Mater.* **2010**, *9*, 345–352.

